Application of a flamelet-based CFD combustion model to the LES simulation of a diesel-like reacting spray

J.M. Desantes [a], J.M. García-Oliver [a], R. Novella [a], E.J. Pérez-Sánchez [b,*]

[a] *CMT - Motores Térmicos, Universitat Politècnica de València*
Edificio 6D, Camino de Vera s/n, 46022, Valencia, Spain
Tel. (0034) 96 387 76 50 / Fax (0034) 96 387 76 59

[b] *Barcelona Supercomputing Center - Centro Nacional de Supercomputación*
Nexus II Building, C/ Jordi Girona 29, 08034, Barcelona, Spain
Tel. (0034) 93 413 77 16 / Fax (0034) 93 413 77 21

Abstract

ECN Spray A, representative of diesel-like sprays, is modelled in the frame of Large-Eddy Simulations (LES) with a Dynamic Structure (DS) turbulence model in conjunction with an Unsteady Flamelet Progress Variable (UFPV) combustion model. In this work, the spray flow field is first calibrated under inert conditions against experimental data. In a second step, the reactive spray is simulated in order to describe flame internal structure when varying ambient temperature. The model shows a good agreement with experimental results and describes the trends observed in flame global parameters, such as ignition delay (ID) and lift-off length (LOL). Low fluctuations are observed in LOL positioning revealing an intense chemical activity at the height of the base of the flame, which stabilizes the reaction in spite of turbulent fluctuations. The analysis of the LES instantaneous fields shows how ignition kernels appear upstream of the base of the flame, clearly detached from the reaction zone, and they grow and merge with the main flame in agreement with previously reported experimental and modelling results. The ambient temperature has a clear impact on the flame structure described by the model and the whole set of results reveal that the UFPV in the frame of LES simulations is suitable for the calculation of diesel

*Corresponding author. Email: eduardo.perez@bsc.es

flames.

Keywords: Large-Eddy Simulation, Spray A, non-premixed flames, chemical mechanism

1. Introduction

The ever-increasing relevance of the transport and energy sectors in our society has lead to the optimization of combustion devices in order to increase their efficiency and reduce pollutant emissions. In particular, understanding the complex phenomena involved in diesel-like reacting sprays and how they interact is a challenging field in the research of partially premixed and non-premixed combustion. These phenomena could be summarized in atomization and break-up, evaporation, mixing, chemical oxidation and spray-wall interaction occurring in a high Reynolds turbulent flow [1].

The complete resolution of the whole physical and chemical processes developing in so different spatial and temporal length scales leads to an unaffordable computational cost and, consequently, different hypothesis have to be introduced in order to derive simplified models. However, these assumptions entail new uncertainties that have to be verified. Unfortunately, measuring in an engine is a difficult task that, in general speaking, only provides global or integral variables insufficient to give an exact picture of the whole combustion process and validate the models.

In this context, the Engine Combustion Network (ECN) [2] has suggested a set of representative experiments to be carried out in special combustion chambers, constant-volume pre-burn (CVP) combustion vessels and constant-pressure flow (CPF) rigs [3, 4], that discard different uncertainties and allow to measure with the most advanced experimental techniques. The empirical observations are complemented with Computational Fluid Dynamics (CFD) simulations. The participation of a wide sector of the researcher community allows to diffuse and improve the state of the art.

In line with this goal, this work deals with simulating the well-known spray

A from ECN, a single nozzle spray with boundary conditions corresponding to modern diesel-like sprays. Liquid length, vapour penetration and some relevant spatial fields together with ignition delay (ID), lift-off length (LOL) are measured in these combustion chambers. A CPF rig is available at CMT-Motores Térmicos whose experimental results are used along this paper [5, 6] unless otherwise stated.

Regarding to diesel spray modelling an extensive literature may be found for inert and reactive conditions. As mentioned previously, the great variety of physical and chemical phenomena occurring at different scales in the flow has given raise to the formulation of many different models aiming to describe these phenomena with different levels of accuracy and computational cost.

For years, the Reynolds Averaged Navier-Stokes (RANS) equations, where the flow is averaged in time for statistically stationary flows or between realizations for transient flows, have been widely used due to their relative reduced computational cost compared to other approaches. Excellent results have been reported for both inert [7] and reactive [8, 9, 10] diesel sprays by means of RANS simulations. Notwithstanding, and despite the positive capabilities of the RANS approach, as the whole range of scales are modelled the hypotheses introduced to develop the models may not be completely fulfilled.

In order to solve more accurately the flow, Large-Eddy Simulations (LES) have gained attention during the last years since, in spite of their higher computational cost, the large eddies are solved and only the smallest scales have to be modelled leading to the development of more accurate models [11]. Contrarily to the larger eddies, which are the most energetic and are strongly affected by the geometry and the boundary conditions of the flow, the universal equilibrium range tends to show statistical isotropy and universality [12] and, hence, is expected that the predictions of the model improve since only the smallest eddies are modelled.

In the case of free shear flows, e.g. jets and sprays, the transport phenomena are mainly controlled by the motion of the large scales which are solved in an LES simulation [13]. Nevertheless, chemical reactions occur when the species

are mixed at molecular level implying that combustion takes place at or even below the smallest scales of the flow. Hence, the LES simulation does not solve the chemical source term which is completely modelled [13, 14]. This leads to directly extend the RANS combustion models to the LES approach. Although, at first glance it may seem that there is not clear advantage in using LES simulations to predict combustion, that is not the case since, as previously mentioned, the integral scales are better predicted and, hence, the scalars predictions are improved.

These scalars are of critical importance specially for combustion models based on conserved scalars, such as the flamelet model. Additionally, other aspects, such as the shape of the filter probability density function (FPDF), have less impact on the final results than in RANS simulations because the mixture is partially solved [14]. Finally, LES simulations make possible to observe intermittency phenomena, which may be critical in the design of combustion devices [15].

The LES formulation is based on the concept of filtering the fields with a filter function G defined as a function of a characteristic length, the filter size Δ, which is usually equal or a multiple of the mesh cell size. G verifies the normalization condition and provides at each point of a general instantaneous field $f(\vec{x},t)$ a filtered field $\widetilde{f}(\vec{x},t)$ (mass-weighted Favre filtering). Then the instantaneous field is decomposed as $f = \widetilde{f} + f''$ where the spatial and temporal dependencies have been omitted. Filtering the instantaneous equations leads to filtered equations where the unresolved fluxes, $\tau_{ij}^{sgs} = \widetilde{u_i u_j} - \widetilde{u}_i\widetilde{u}_j$ and $\phi_i^{sgs} = \widetilde{\phi u_i} - \widetilde{\phi}\widetilde{u}_i$, as well as filtered source terms are computed with the turbulence model and additional closures [11].

Different turbulence models may be found in the literature which use different approaches to estimate the values of the unresolved fluxes. The models based on the Boussinesq hypothesis require the definition of a sub-grid scale viscosity and are classified as viscosity models as a distinction from the non-viscosity models that do not use such hypothesis.

The Smagorinsky model is a viscosity model and was the first used for LES.

The sub-grid scale viscosity ν_{sgs} is proportional, by means of a positive constant C_S, to the square of the filter size and the resolved strain rate. However, constant C_S may change with the Reynolds number (near wall region) and the flow configuration and no backscatter is allowed [11, 15]. In order to avoid this problem the dynamic model was proposed by Germano et al. [16] where the constant C_S is computed for each cell from the resolved field.

The previous models do not require additional transport equations and, hence, it is expectable that the predictions improve if a variable that characterizes the turbulent state, like the sub-grid kinetic energy k_{sgs}, is transported. This gives raise to the One Equation Eddy model (OEE) which defines ν_{sgs} from the transported sub-grid kinetic energy [17]. Modelling more accurately the sub-grid interactions allows to use coarser meshes which are more compatible with Lagrangian droplet models, conventionally used to model the liquid phase in spray simulations. Again the dynamic procedure may be applied in conjunction with the OEE to improve the results.

In the Dynamic Structure model (DS), which is a non-viscosity model, the residual stress fluxes τ_{ij}^{sgs} are considered proportional to the sub-grid turbulent kinetic energy by means of a coefficient tensor [18]. Applying this scaling at two different filter levels these coefficients may be written as a function of the Leonard stress tensor. Additionally, a transport equation for k_{sgs} is required. This model fulfils some important properties that are desirable for any turbulence model. Due to its capabilities to perform accurate simulations it has been adopted in the current work [19, 20].

Solving a diesel spray simulation requires a combustion model with the ability of managing complex chemical schemes while retaining turbulence-chemistry interaction (TCI). Between the different models available in the literature the flamelet-based model appears as one of the most promising alternatives [21, 22, 23, 24, 25, 8] with a remarkable balance between accuracy and computational cost. These models describe the turbulent flame as an ensemble of strained laminar flames called flamelets [26]. The flamelet equations may be rewritten in the mixture fraction space yielding a system of one-dimensional transport

equations [27, 28]. In LES framework, the solutions provided by this system are integrated by means of FPDFs in order to account for the TCI.

Depending on the approach, the flamelet equations may be solved during the CFD calculation, as in the Representative Interactive Flamelet model (RIF) [29], or, on the contrary, the flamelet solutions may be pre-tabulated, following the Intrinsic Low Dimensional Manifold (ILDM), as in the Flamelet Generated Manifold (FGM) [21] or the Flame Prolongation of ILDM (FPI) [30]. This last approach is adopted in this work.

However, despite the advantages provided by these models the computational cost may increase exponentially when dealing with diesel engine simulations where the boundary conditions may span over wide ranges [31, 32]. In this context, a simplified approach called Approximated Diffusion Flamelets (ADF) was suggested in order to reduce drastically the computational cost while retaining the ability to manage complex chemistry [31]. This approach is adopted for the current work given the reported excellent results provided in the literature [33, 25, 32, 10].

2. Problem description

The objective of this work is the simulation of spray A in the LES framework by means of the flamelet concept. The boundary conditions for spray A are reproduced in table 1 corresponding to a temperature parametric sweep. Nominal injector diameter is 90 μm, with nozzle code 210675 [2] and discharge coefficient equal to 0.9 [34]. The fuel is n-dodecane which is used as a diesel surrogate. A long injection mass rate ($\geq$ 4 ms) with an injection pressure p_{inj} of 150 MPa is imposed [35] where the temperature fuel is assumed equal to 363 K. In table 1 the values for the stoichiometric and saturation mixture fractions, Z_{st} and Z_s, respectively, are included. The value for Z_s corresponds to the maximum mixture fraction value in the air-fuel mixture for which fuel does not condensate and is calculated from a mixing-controlled approach [36].

The CFD simulation is carried out in the open CFD platform Open Foam

Table 1: Definition of spray A parametric study.

X_{O2}	T_{amb} (K)	ρ_{amb}(kg/m^3)	p_{amb} (MPa)	p_{inj} (MPa)	Z_{st}	Z_s
0.15	750	22.8	4.97	150	0.046	0.251
0.15	800	22.8	5.3	150	0.046	0.278
0.15	850	22.8	5.63	150	0.046	0.303
0.15	900	22.8	5.96	150	0.046	0.326

environment [37] with an in-house developed code. The mesh is a cylinder composed of approximately 3.6 Million cells with a definition in terms of cell size and distribution based upon the spray geometry. The cylinder has a radius of 23.5 mm and height of 108 mm with open boundary conditions for all the faces except the base of the cylinder, where the injector is positioned, which is a wall. The mesh is composed of an internal prism with its axis coincident with the cylinder one. The length of its base measures 1.688 mm and is composed of square cells with a constant size of 62.5 μm, following the recommendation given in the literature for the use of Lagrangian droplet models [38, 39]. The rest of the mesh follows a discretization in cylindrical coordinates with 108, 108 and 292 cells in radial, azimuthal and axial directions, respectively, and an expansion ratio between cells of 1.015 for the radius and 1.01 for the axial distance. Different views and cuts of the mesh are shown in figures 1 and 2.

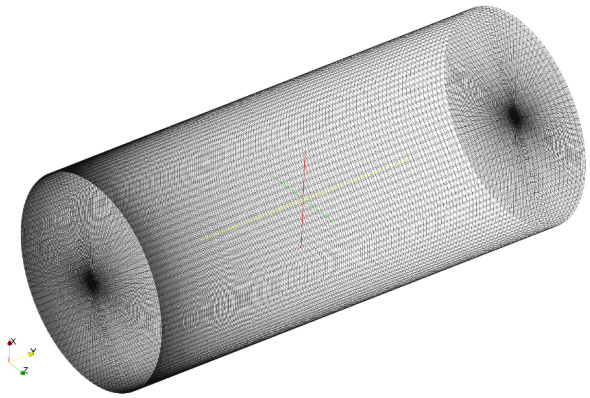

Figure 1: 3D view of the mesh and the domain.

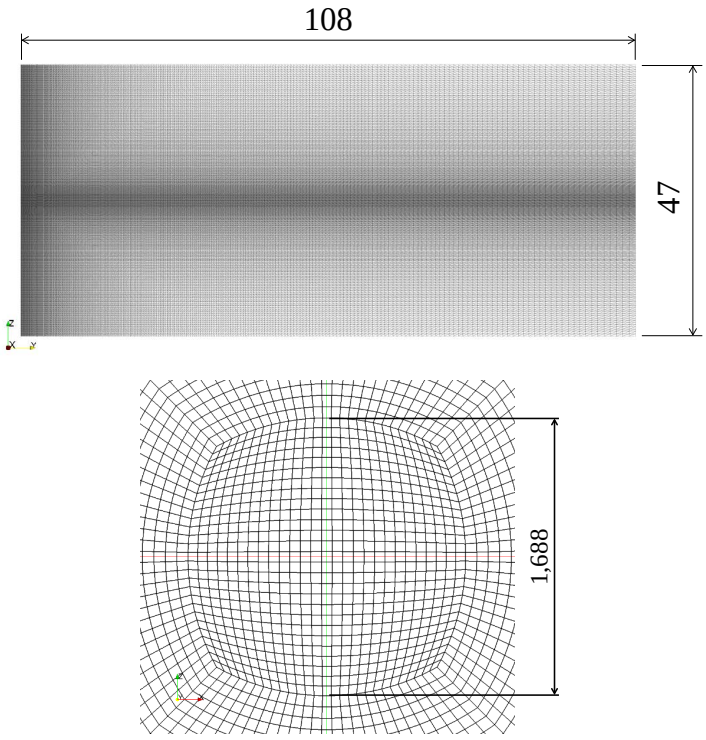

Figure 2: Different cuts of the mesh used for the calculations. Left figure shows a meridian plane. Right figure shows a perpendicular cut to the cylinder axis with a zoom at the inner prism. Dimensions in mm.

A DS model has been adopted to solve the residual stresses in the diesel spray simulation in the formulation described in [19, 40] and the implementation given in [20], which accounts for the sub-grid interactions between the gas phase and the fuel droplets. For these droplets a Lagrangian approach has been used with the Reitz model [41] that accounts for the Kelvin-Helmholtz/Rayleigh-Taylor instabilities. The droplets are injected following a Rosin-Rammler distribution where the droplet diameter ranges from 10 μm to the diameter of the nozzle. The evaporation is solved with a Ranz-Marshall correlation and the collision is treated with the O'Rourke model.

The combustion model is based on the flamelet concept where the set of laminar flamelets are solved in the mixture fraction Z space. According to the

theory devised by Peters [27, 28], for each flamelet a system of partial differential equations (PDEs) is solved, that accounts for the transport phenomena, in conjunction with the ordinary differential equations (ODE) system for the chemical source terms. The flamelet equation reads for each species

$$\frac{\partial Y_k}{\partial t} = \frac{\chi}{2}\frac{\partial^2 Y_k}{\partial Z^2} + \dot{\omega}_k \qquad k = 1, \ldots, N \tag{1}$$

where Y_k is the species mass fraction for species k and N is the total number of species. The scalar dissipation rate χ measures the diffusivity in the Z space and is prescribed following the profile

$$\chi(a, Z) = \frac{a}{\pi} Z_s^2 \exp[-2(\mathrm{erfc}^{-1}(2Z/Z_s))^2] = \chi_{st}\frac{F(Z)}{F(Z_{st})} \tag{2}$$

where subscript st refers to stoichiometric values and a is the strain rate [28]. The set of equations given by the system (1) with the chemical ODE system can be unaffordable when solving complex chemical mechanisms and a wide set of boundary conditions, as found for diesel engines simulations.

Based on these limitations the ADF model was suggested in order to deal with complex mechanisms in reduced computational times when solving the flamelet equation [31]. In this approach only the progress variable Y_c equation is solved, where Y_c is defined as a linear combination of species mass fractions. The chemical source terms as well as the relationships between the species and Y_c come from solving a set of homogeneous reactors (HRs). This leads to solve first the corresponding set of HRs, which are not computationally expensive, where the initial conditions come from the adiabatic mixing between the air and the fuel with the corresponding boundary conditions [36]. In this work this has been done with Chemkin software [42]. Then the flamelet equation reads

$$\frac{\partial Y_c}{\partial t} = \frac{\chi(a,Z)}{2}\frac{\partial^2 Y_c}{\partial Z^2} + \dot{\omega}_c^{HR}(Z, Y_c) \tag{3}$$

where the dependencies are explicitly written. This approach has been adopted to solve spray A in this work and its implementation has been carried out following [43].

The steady solutions are first computed with a Newton-Rapson algorithm and then the unsteady solutions are calculated with an implicit method and an adaptive time step algorithm based on the chemical source term. Second order is used for mixture fraction derivatives while first order for temporal derivatives.

Once the flamelet equations are computed a database in the form $\psi = \psi(Z, \chi_{st}, t)$ is available where ψ is any reactive scalar. The TCI, necessary to model the sub-grid effects of the turbulence, is accounted for by means of FPDFs. A beta function is used in the mixture fraction direction [28], defined by $(\widetilde{Z}, \widetilde{Z''^2_{sgs}})$ where $\widetilde{Z''^2_{sgs}}$ corresponds to the sub-grid mixture fraction fluctuations, while for the rest of variables δ-functions are assumed. Additionally, statistical independence is hypothesized leading to

$$\widetilde{\psi}(\widetilde{Z}, \widetilde{Z''^2_{sgs}}, \widetilde{\chi_{st}}, \widetilde{t}\,) = \int_0^{\infty}\int_0^{Z_s}\int_0^{\infty} \psi(Z, \chi_{st}, t)\, \delta(t - \widetilde{t}\,)\, P_Z(Z, \widetilde{Z}, \widetilde{Z''^2_{sgs}})\, \delta(\chi_{st} - \widetilde{\chi_{st}})\, \mathrm{d}t\, \mathrm{d}Z\, \mathrm{d}\chi_{st} \tag{4}$$

which becomes

$$\widetilde{\psi}(\widetilde{Z}, \widetilde{Z''^2_{sgs}}, \widetilde{\chi_{st}}, \widetilde{t}\,) = \int_0^{Z_s} \psi(Z, \widetilde{\chi_{st}}, \widetilde{t}\,)\, P_Z(Z, \widetilde{Z}, \widetilde{Z''^2_{sgs}})\, \mathrm{d}Z \tag{5}$$

Equation (5) is reparametrized as $\widetilde{\psi} = \widetilde{\psi}(\widetilde{Z}, \widetilde{Z''^2_{sgs}}, \widetilde{\chi_{st}}, \widetilde{Y_c})$ providing a turbulent solution manifold. In the same way the χ profile is integrated yielding a relationship in the form

$$\widetilde{\chi} = \widetilde{\chi_{st}}\, J(\widetilde{Z}, \widetilde{Z''^2_{sgs}}) \tag{6}$$

In this work, around 32 values have been tabulated for $\widetilde{Z}$, 17 for $\widetilde{Z''^2_{sgs}}$, 35 for $\widetilde{\chi_{st}}$, depending on the boundary conditions, and 51 for $\widetilde{Y_c}$ with a parabolic distribution in order to retain accurately the auto-ignition.

Continuity, Navier-Stokes and energy equations are solved together with the sub-grid kinetic energy. Additionally, the most important species (H, OH, CO, CO_2, H_2O, $C_{12}H_{26}$, CH_2O, C_2H_2, C_7H_{14}, H_2, O_2, N_2) are transported [44] and the set of species chemical source terms $\widetilde{\dot{\omega}_k}$ is computed from the turbulent flame manifold. For such purpose, transport equations for $\widetilde{Z}$ and $\widetilde{Z''^2_{sgs}}$ have to be solved. In the $\widetilde{Z''^2_{sgs}}$ equation the sub-grid dissipation term is modelled by [33, 25]

$$\widetilde{\chi_{sgs}} = C_\chi D_{sgs} \frac{\widetilde{Z''^2_{sgs}}}{\Delta^2} \tag{7}$$

D_{sgs} is the sub-grid mass diffusivity defined from ν_{sgs} with a Schmidt number 0.7 [19] and C_χ is a constant to be adjusted. The total scalar dissipation rate is $\widetilde{\chi} = \widetilde{\chi_{sgs}} + 2D|\nabla \widetilde{Z}|^2$, with D the laminar mass diffusivity, which is related to $\widetilde{\chi_{st}}$ by the pair $(\widetilde{Z}, \widetilde{Z''^2_{sgs}})$ by means of equation 6.

From the transported species mass fractions the $\widetilde{Y_c}$ is obtained, which is defined as $\widetilde{Y_c} = \widetilde{Y_{CO}} + \widetilde{Y_{CO_2}}$ [31]. With the input parameters $(\widetilde{Z}, \widetilde{Z''^2_{sgs}}, \widetilde{\chi_{st}}, \widetilde{Y_c})$ the source term for $\widetilde{Y_c}$, $\partial \widetilde{Y_c}/\partial t$, obtained from solving the flamelets and integrating, is retrieved and used to obtain the $\widetilde{Y_c}$ at next time step due to chemical effects according to the following expression

$$\widetilde{Y_c}(t + \delta\tau) = \widetilde{Y_c}(t) + \frac{\partial \widetilde{Y_c}}{\partial t}(\widetilde{Z}, \widetilde{Z''^2_{sgs}}, \widetilde{\chi_{st}}, \widetilde{Y_c}(t))\, \delta\tau \tag{8}$$

where the different values are taken in each cell of the domain. From $(\widetilde{Z}, \widetilde{Z''^2_{sgs}}, \widetilde{\chi_{st}}, \widetilde{Y}_c(t+\delta\tau))$ and the corresponding tabulation, the species mass fractions $\widetilde{Y_k}^{tab}$ are also retrieved, enabling the calculation of the source term $\widetilde{\dot{\omega}_k}$ according to the following equation.

$$\widetilde{\dot{\omega}_k} = \frac{\widetilde{Y_k}^{tab}(\widetilde{Z}, \widetilde{Z''^2_{sgs}}, \widetilde{\chi_{st}}, \widetilde{Y}_c(t+\delta\tau)) - \widetilde{Y_k}}{\delta\tau} \tag{9}$$

where $\widetilde{Y_k}$ is the mass fraction for species k at the cell. $\delta\tau$ is the time step for advancing in the chemical manifold which is taken equal to the CFD time step, fixed to 0.02 μs.

The flow is solved by means of the finite volume method. To solve the transport equations the PIMPLE algorithm is applied where the temporal derivatives and the Laplacian terms are evaluated with second order schemes and the divergence is computed from the fluxes with a blended difference that combines the upwind and central differencing with the same weight.

For the current calculations, the dodecane oxidation is described by the chemical scheme developed by Narayanaswamy et al. [45] which comprises 255 species and 2289 reactions, which is widely extended in the literature [46, 47].

3. Results and discussion

The analysis is divided in a first section where the model is validated in terms of the nominal inert and reactive spray and a second part devoted to the description of reactive spray and how is influenced by the boundary conditions.

3.1. Validation of the model

The spray is first calibrated at inert conditions for the nominal condition by means of modelling and experimental data comparison. As a preliminary step, the vapour penetration and the liquid length for the simulated and the experimental results [6] are shown in figure 3. The liquid length is defined as the distance to the nozzle where 95% of the injected liquid is found and the

vapour penetration is given by the maximum distance from the nozzle outlet to where mixture fraction is 0.001 [2].

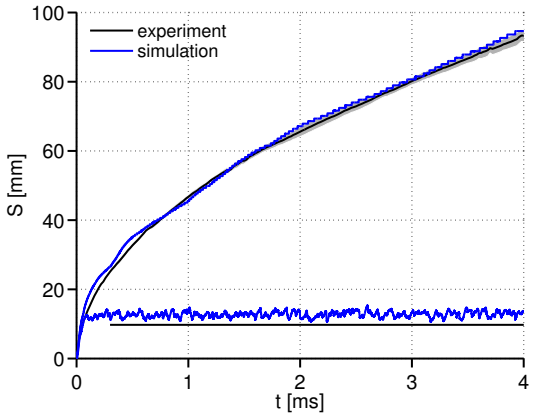

Figure 3: Vapour penetration and liquid length for experimental and simulated inert nominal condition. For experiments, uncertainty of measurements is delimited with shadows.

Although the liquid length is slightly overestimated an excellent agreement is observed for the spray vapour penetration since simulated and experimental curves fall very close.

The validation of the simulation is followed by the comparison of the mean mixture fraction, $\langle \widetilde{Z} \rangle$, its standard deviation, $\sqrt{\langle \widetilde{Z''^2} \rangle}$ or Z_{rms}, and the mean axial velocity $\langle \widetilde{U} \rangle$ normalized by the velocity at the exit of the nozzle. The symbol $\langle\,\rangle$ denotes averaged value. These profiles obtained from the simulation are averaged in time and azimuthal directions and are compared with experimental results in figure 4. The measurements were obtained by means of Rayleigh imaging for the mixture fraction and Particle Image Velocimetry (PIV) for the velocity [48, 49, 50, 51]. As the measurements and the simulations have been carried out with different nozzles the distances are normalized by the equivalent diameter $d_{eq} = d_0\sqrt{\rho_f/\rho_a}$ where d_0 is the nozzle diameter and ρ_f, ρ_a are the fuel and air densities, respectively. The radial cuts at 50 and 90 d_{eq} correspond to axial distances of 25 and 45 mm, approximately.

An excellent agreement is observed for $\langle \widetilde{Z} \rangle$ and $\langle \widetilde{U} \rangle$. For Z_{rms}, an analysis of the constant C_χ shows that it has no strong impact on the results. Notwith-

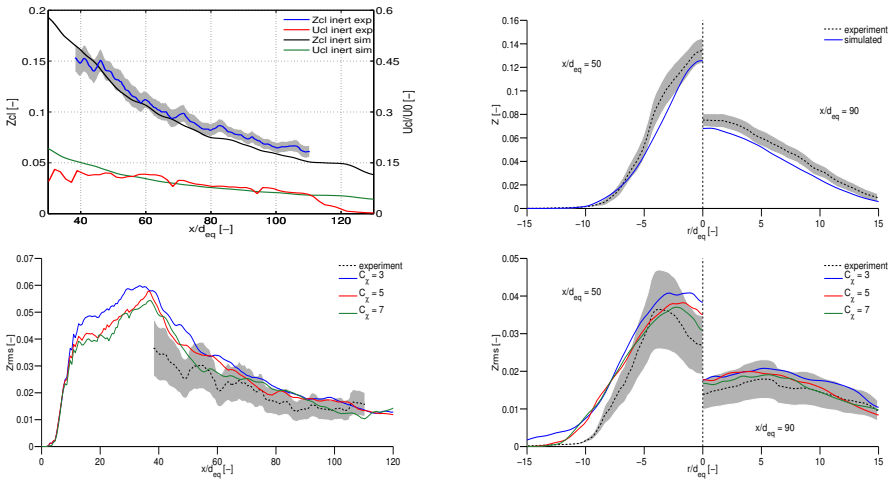

Figure 4: Spray validation for very advanced time instants. Top left: $\langle \widetilde{Z} \rangle$ and normalized $\langle \widetilde{U} \rangle$ on the centerline. Top right: $\langle \widetilde{Z} \rangle$ radial profiles at 50 and 90 d_{eq}. Bottom left: Z_{rms} on the centerline for different C_χ values. Bottom right: Z_{rms} radial profiles at 50 and 90 d_{eq} for different C_χ values. Experimental uncertainties delimited with shadowed regions. Results for nominal inert condition.

standing, it is observed a slight decrease of Z_{rms} when increasing the C_χ constant and, finally, a value of $C_\chi = 5$ has been chosen to calibrate the model. With this value the experimental profiles for Z_{rms} are reasonably well-captured on the axis and the radial cuts.

Finally, the energetic spectral content of turbulence is gathered in figure 5 for two points on the axis and other radially displaced for the nominal inert case. The energy spectrum is obtained in the frequency domain, following [52], from the axial velocity signal registered at a given point during a temporal window where the turbulent statistics stabilize. Then the velocity autocorrelation function is computed and the Fourier transform is applied for this function providing the energy spectrum.

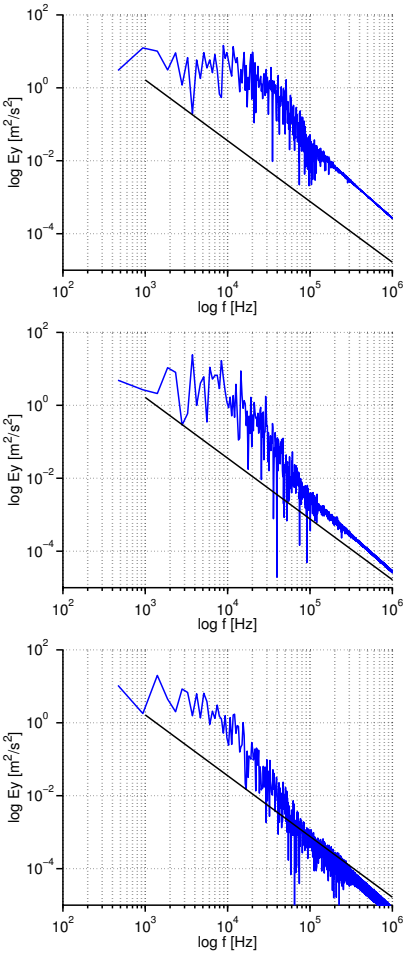

Figure 5: Energy spectrum in the frequency domain for points on the axis at a distance of 20 (top) and 30 mm (center) and a 2 mm radially displaced point positioned 30 mm from the nozzle (bottom). For reference a straight line with slope -5/3 is included too. Results for nominal inert case.

From figure 5 is clearly seen that there exists a range of frequencies where the spectrum is almost flat corresponding to the integral scales of the flow. In spite of the noise in the signal, the energy spectrum is observed to fall in the high frequency range with a slope close to the value -5/3 predicted by the classic turbulence theory, which corresponds to the inertial sub-range [12, 11]. This range is positioned in frequencies between 10^4 and 10^5 Hz. Besides, figure 5

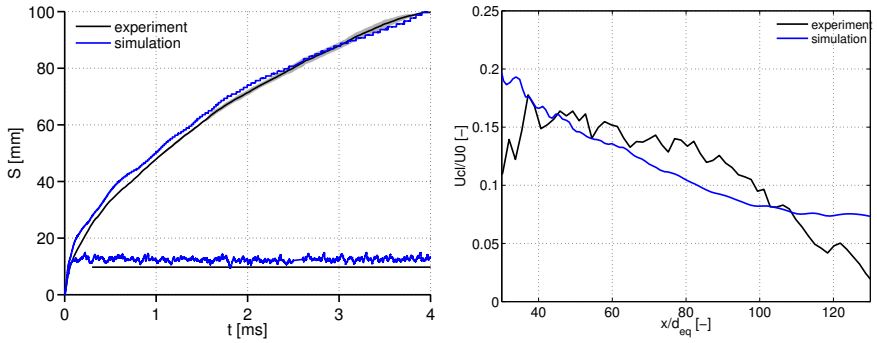

Figure 6: Left figure: tip penetration and liquid length for experimental and simulated reactive nominal condition. For experiments, uncertainty of measurements is delimited with shadows. Right figure: normalized $\langle \widetilde{U} \rangle$ on the centerline.

shows that when moving away from the nozzle on the axis or radially away from the axis, the inertial sub-range tends to shift towards lower frequencies, which implies that the flow dynamics become slower as a result of the reduction of the velocities.

In general, this range intends to be partially or completely solved with LES simulations. It is worth mentioning that it is probable that the current simulations do not solve completely the inertial sub-range because of the large cell sizes that the DDM formulation forces in order to fulfil its hypotheses. As previously said, in this work a minimum cell size of 62.5 μm has been imposed following the results obtained in the literature for diesel sprays when using the DDM approach [38, 39].

The calibration of the inert spray is considered quite satisfactory and it encourages the validation of the spray in reactive conditions. Again this is done by the comparison of modelling and experimental data for the reactive nominal case. Figure 6 gathers the comparison of the tip penetration and the liquid length as well as the axial velocity on the axis normalized by the velocity at the exit of the nozzle. The tip penetration for the reactive case is defined in a similar way that the vapour penetration, that is, the maximum distance from the nozzle outlet to where mixture fraction is 0.001.

Figure 6 shows that there exists an excellent agreement for the tip pene-

tration. Regarding the liquid length is slightly overestimated as in the inert condition. However, as the liquid region is spatially isolated from the flame due to spray A boundary conditions it is expected that this overestimation does not influence subsequent results. Finally, the axial velocity on the axis from the simulation shows an acceptable correspondence with experimental results.

The validation of the model is closed with a qualitative comparison of formaldehyde (CH_2O) and hydroxide (OH) fields with measured Laser Induced Fluorescence (LIF) data from [51] at advanced instants for the reactive nominal case. Experimental results are averaged in time and, consequently, are compared with averaged LES simulations results. Additionally, for the sake of completeness, instantaneous snapshots for the LES simulation are included too. Since the nozzle diameter in experiments is slightly different from that used for the calculation, the distances are again normalized by the equivalent diameter. These results are gathered in figure 7.

CH_2O is detected in the vicinity of the LOL in both experimental and simulated results. In the first case, the signal has been saturated downstream of 50 d_{eq} in order to better visualise the CH_2O field since, as discussed in [51], this downstream signal is probably due to the interference of polycyclic aromatic hydrocarbons (PAHs). LES simulation predicts a narrow region of CH_2O production in the zone of rich mixtures close to the LOL and positioned in the axial distance of 30-50 d_{eq} in agreement with experimental results.

It is observed that in the experiment the CH_2O field seems to extend upstream of the measured LOL while in the simulation it appears downstream of the LOL from the CFD. It is difficult, however, to extract a conclusion from this fact since the LOL definitions for experiments and simulations are not exactly the same and this comparison is intended to be only qualitative and, hence, some discrepancies are expected to arise.

Regarding the OH field the simulation predicts two regions of OH production in a similar way than the experiment although in the experiment OH spreads over a wider region. In both cases OH is produced downstream of the corresponding LOL position. In the experiment the laser sheet extends until 92 d_{eq},

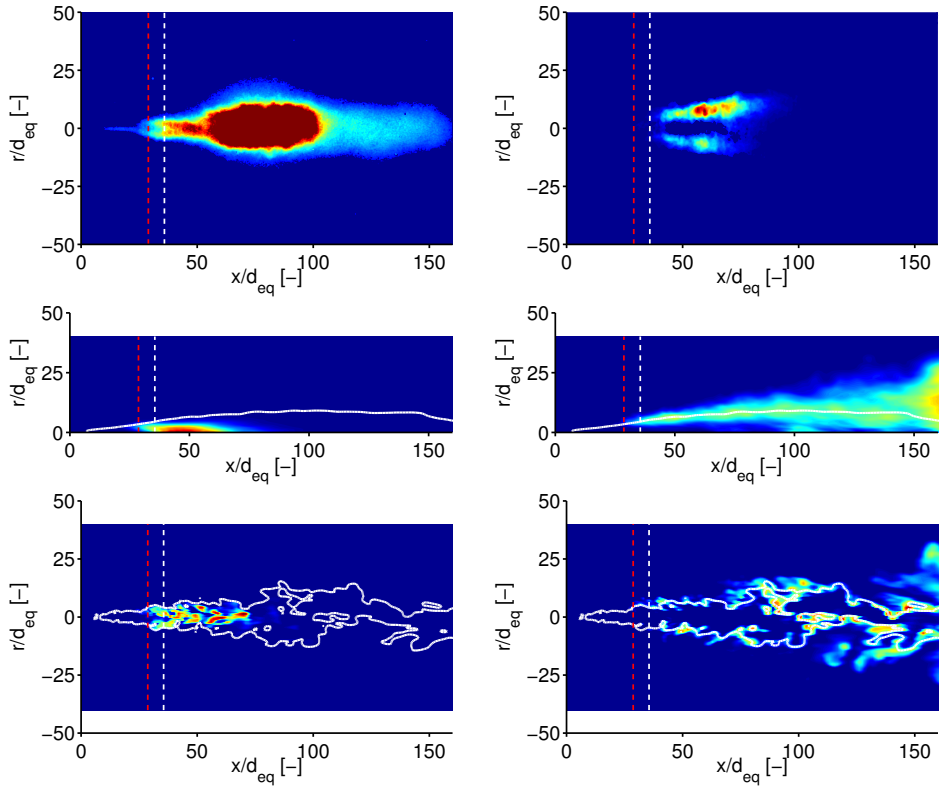

Figure 7: Comparison of the CH_2O and OH fields for the nominal case. First row correspond to experimental results [51], second row is for LES averaged solutions and third row is for instantaneous LES simulation snapshots. Left column shows 355 nm LIF signal for the experiment and the CH_2O field for the simulation while right column is derived from OH LIF signal for the experiment and shows the OH field for the simulation. LOL values for experiment (white dashed) and simulation (red dashed) are shown and the stoichiometric level curve is included for the modelled results.

approximately, and no further information is available.

The results obtained so far show that there exists a good agreement between the LES simulations in inert and reactive conditions and the experiments and, hence, this enables the analysis of the reactive spray.

3.2. Analysis of the reactive flame

The analysis of the reactive spray is carried out in terms of flame metrics, namely ID and LOL, and reactive scalar fields in spatial and mixture fraction-temperature (Z-T) space representations for the different boundary conditions.

3.2.1. Global parameters

First, the ID and LOL for the temperature sweep are shown in figure 8. The ID is defined as the time spent from start of injection (SOI) until the maximum Favre filtered ambient temperature increases 400 K [1]. For the LOL a first definition, following the ECN criterion, has been adopted [2], which defines this value as the minimum axial distance from the nozzle to the surface level given by the averaged Favre filtered OH mass fraction corresponding to the 14 % of the maximum value reached in this field. This LOL value is labelled as 'LES OH aver.' in figure 8. However, a second definition for the LOL has been considered which is computed as the average of the minimum axial distance from the nozzle to the surface level of the Favre filtered OH mass fraction corresponding to the 14 % of the maximum value reached in this field. This value is labelled as 'LES OH instant.' in figure 8. This will make possible to evaluate the impact of the order of the operations in defining the LOL.

Representative values for $\widetilde{Y_{\mathrm{OH}}}$ are found in the vicinity of the stoichiometric mixture fractions where the temperature is maximum. However, during the injection rate, which lasts for 4 ms, the surface levels for $\widetilde{Z} = Z_{st}$ do not stabilize completely making difficult to obtain representative averaged $\widetilde{Y_{\mathrm{OH}}}$ fields and, particularly, the maximum value. Consequently, as the first methodology (ECN criterion) first averages the $\widetilde{Y_{\mathrm{OH}}}$ field this may cause some uncertainties in the LOL value and as a consequence of these shortcomings a second definition for the LOL has been suggested.

As observed in figure 8 there exists an excellent agreement between ID results for all the temperatures except for the lowest one, for which the LES simulation predicts a too fast ignition. Regarding the LOL, both criteria provide similar results although a slight deviation is accentuated when decreasing the reactivity. Moreover, both definitions give short LOL values although they reproduce the expected trends. The LOL values for the second definition ('LES OH instant.') seem to show a clearer parallelism to the experimental curve than the first one ('LES OH aver.').

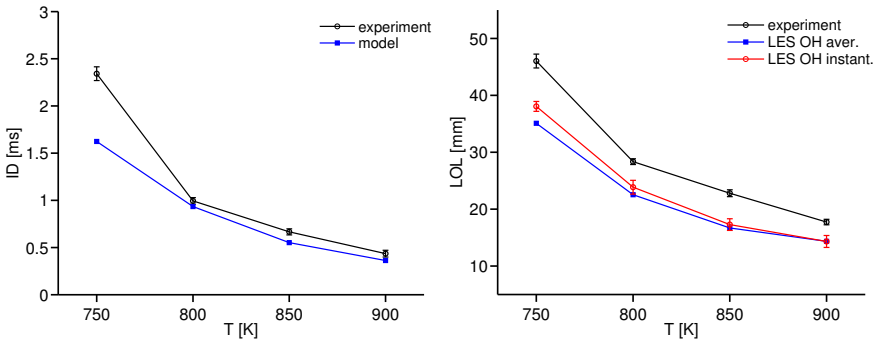

Figure 8: Ignition delay (left) and lift-off length (LOL) (right) for the temperature parametric sweep. Error bars delimit the standard deviation of the variable.

In addition, the standard deviation has been computed for the second definition and included in the figure by means of error bars. This fluctuation is computed from the resolved motions and does not consider a sub-grid component. However, it is thought that this fact does not modify subsequent conclusions. It is observed that the fluctuation level is not very high in agreement with the experimental results which are of the same order of magnitude (± 1 mm) than those corresponding to the simulations.

In order to visualize how the LOL evolves in time, figure 9 shows the temporal evolution of the LOL computed with the instantaneous $\widetilde{Y_{\mathrm{OH}}}$ field. The LOL value computed with the first criterion is included too.

From figure 9 it arises that the first ignition kernels appear at positions downstream the distance where the LOL finally stabilizes since the LOL position moves upstream during the first steps of the ignition, as reported in other works [1, 53]. The fluctuations related to the LOL are low (± 1 mm) and do not depend clearly on the ambient temperature.

Moreover, the LOL position signal shows rapid and strong fluctuations, similar to discontinuities, when it stabilizes, e.g. at 2.7 ms for 900 K or 3.5 ms for 800 K. This is not due to a rapid recession of the base of the flame but to the apparition of ignition kernels that spontaneously start burning upstream and detached from the base flame as will be explained in detail in section 3.2.2.

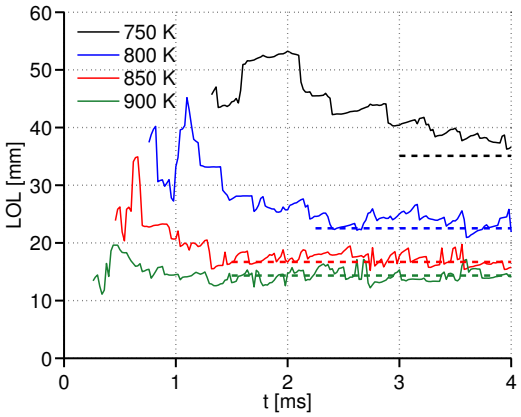

Figure 9: Instantaneous LOL evolutions for the different ambient temperature cases (solid line) and LOL defined with ECN criterion (dashed line).

Therefore, the base of the flame, defined by the LOL position, is anchored in the vicinity of a fixed point and does not experiment high fluctuations implying that the diesel spray generates a stable and vigorous flame. An intense partially premixed flame is established in the vicinity of the LOL where reactants rapidly burn into intermediate products releasing important amounts of heat [54]. This entails that the chemical activity is weak upstream of the LOL but it is triggered at the LOL distance. The intensity of the chemistry is so high that it is not strongly affected by the local flow conditions and then the LOL shows low fluctuations as observed in figures 8 and 9. A deeper insight into the occurrence of such ignition kernels at the LOL distance is developed in next section for the different boundary conditions.

3.2.2. Instantaneous fields

This section shows the instantaneous fields for some important reactive scalars in both spatial and Z-T representations for advanced instants and an analysis of the formation of the ignition kernels at the base of the flame.

Figure 10 gathers the temperature, $\widetilde{Y_{CH_2O}}$ and $\widetilde{Y_{OH}}$, which are tracers of the low and high temperature combustion respectively, for instants 3500, 3800 and 4000 μs.

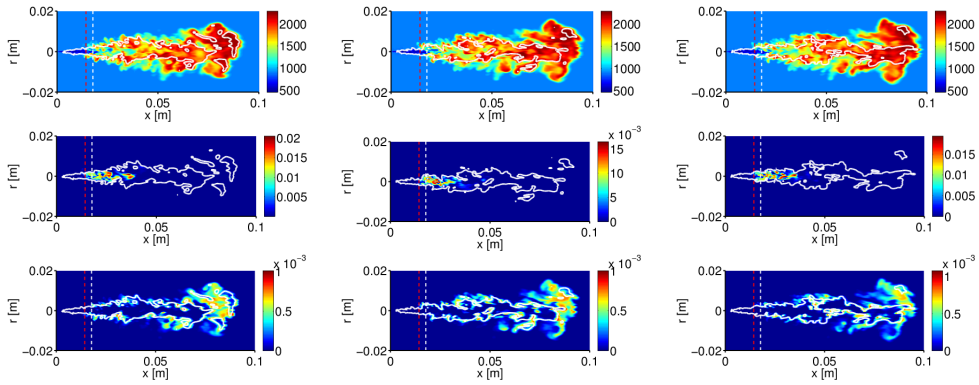

Figure 10: Instantaneous fields for $\widetilde{T}$ (first row), $\widetilde{Y_{\mathrm{CH_2O}}}$ (second row) and $\widetilde{Y_{\mathrm{OH}}}$ (third row) for the instants 3500 (left), 3800 (center) and 4000 μs (right). The level curve $\widetilde{Z} = Z_{st}$ is included in white line. LOL values for experiment (white dashed) and simulation (red dashed) are shown too. Results for nominal case.

The instantaneous fields reveal the structure of the turbulent flame [54], namely, a partially premixed flame positioned at the LOL distance where ignition kernels appear and reactants burn into products reaching temperature values close to 2000 K on the stoichiometric level curve. This premixed flame is radially displaced shaping the flame as two reactive lobes separated by an inert or less reactive mass on the axis due to the richness of its mixture. As the flow moves downstream of the LOL, regions located around the stoichiometric level curve show higher temperatures due to the completeness of the chemical reactions and a diffusion flame is established. At the transient head of the spray, pockets with very high and low temperatures are seen to alternate due to the inhomogeneities of the turbulent flow.

Formaldehyde field shows that this species is produced in the vicinity downstream the LOL as it is a tracer of the low and intermediate temperature reactions. In addition, it is observed how this field is enclosed by the stoichiometric level curve and appears in the rich mixtures region, positioned close to the axis, surrounded and partially overlapped by the partially premixed flame. A high variability is found for this field as is observed in the different instants due to the high velocities found in this region.

Regarding hydroxide, it is found on the stoichiometric surface where very high temperatures are reached and at the transient head of the spray where a wide spatial region shows very high temperatures.

This picture of the flame structure agrees with classical works [54] and recent experimental findings [51].

Moreover, the LES simulation reproduces the small eddies found in the periphery of the spray due to the shear stresses, between high speed spray and quiescent air, responsible of the intense mixing process [55]. A high fluctuation of these eddies is found close to the LOL and its proximities. When moving downstream, the exchange of momentum between the spray and the air due to air entrainment decreases the velocities and increases the characteristic time scales of the eddies. This point is important when obtaining averaged fields and will be further commented in next section.

In line with the fluctuations, a high variability in the stoichiometric level curves is observed between the different instants. The fact that the hydroxide is positioned in the close vicinity of the stoichiometric level curve and the high variability of this curve, induced by the turbulent motions, makes difficult to obtain a representative averaged field for $\widetilde{Y_{\mathrm{OH}}}$ as was mentioned in previous paragraphs. This fact may influence LOL values when computed from averaged fields if the temporal window does not extend during long times.

More insight on the structure of the flame is gained when showing the instantaneous fields in Z-T maps for the nominal case. These maps are represented in figure 11 for the same instants than in figure 10. For a better visualization only points with a mass fraction higher than the 0.25 of the maximum of the field are included. Figure 11 shows the mass fraction fields for $\widetilde{Y_{\mathrm{CH_2O}}}$, $\widetilde{Y_{\mathrm{OH}}}$ and $\widetilde{Y_{\mathrm{C_2H_2}}}$, where acetylene ($C_2H_2$) is a soot precursor.

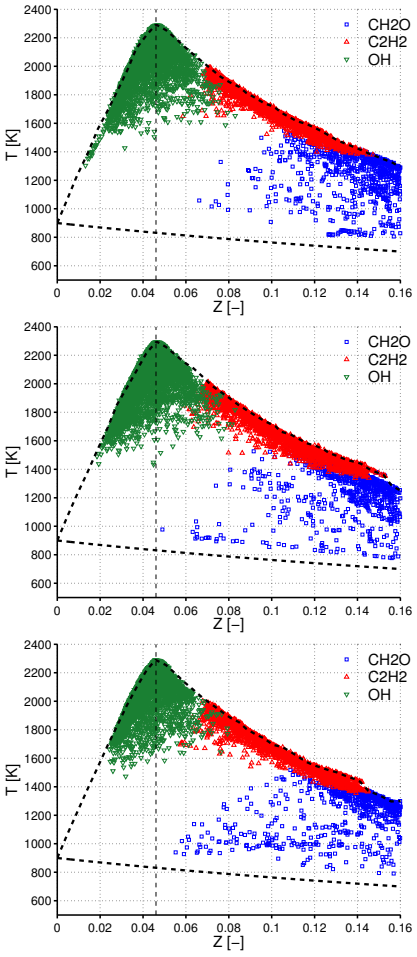

Figure 11: Z-T maps for 3500 (top), 3800 (center) and 4000 μs (bottom) for the $\widetilde{Y_{\mathrm{CH_2O}}}$, $\widetilde{Y_{\mathrm{OH}}}$ and $\widetilde{Y_{\mathrm{C_2H_2}}}$ fields. The adiabatic initial mixing and contour of the map are included with black dashed lines. The stoichiometric value is shown with a vertical line. Results for nominal case.

The maps show that formaldehyde is positioned in the intermediate temperatures and rich mixtures regions while hydroxide appears in the vicinity of the stoichiometric position for very high temperatures out of the equilibrium [56] as was pointed in previous paragraphs. Acetylene is limited to rich mixtures and temperatures close to equilibrium.

In addition, there exists a clear variability between the position and density of the points of the fields in the maps. This is especially marked for the

formaldehyde as was stated when describing the spatial fields, probably due to the high turbulence levels found in the vicinity of the LOL. The contour of the maps shows negligible fluctuations showing that there always exist points at equilibrium in the whole range of reactive mixtures.

A comparison in the Z-T space, similar to that shown in figure 11, for the 750, 800 and 900 K cases is shown in figure 12 for the instantaneous fields. It is observed how the increase of reactivity by means of the ambient temperature enhances the rich mixtures reactivity and rises the maximum temperature reached in the domain. The displacement of combustion towards richer mixtures is of paramount importance for soot formation. Experimentally, it has been found that negligible soot concentration is detected for the 750 K case [3]. In the simulations it is seen that C_2H_2 field spreads on richer mixtures that reach higher temperatures when increasing the ambient temperature and, hence, it is expected that this would lead to higher soot formation.

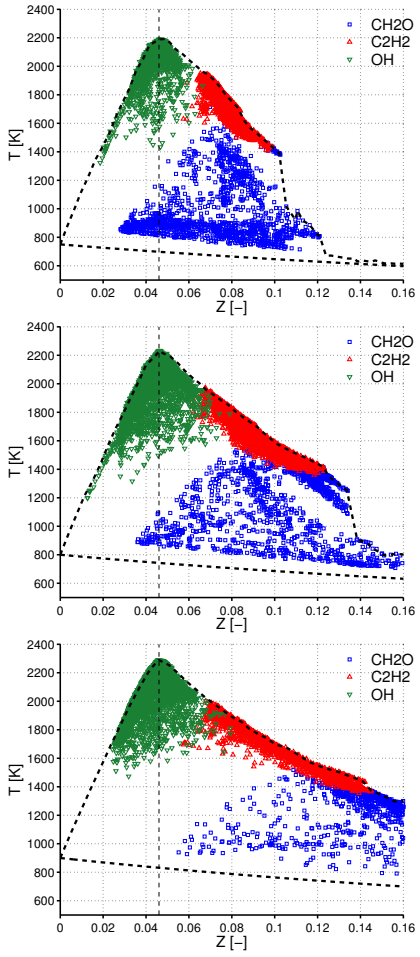

Figure 12: Z-T maps for 750 (top), 800 (center) and 900 K (bottom) for the $\widetilde{Y_{\mathrm{CH_2O}}}$, $\widetilde{Y_{\mathrm{OH}}}$ and $\widetilde{Y_{\mathrm{C_2H_2}}}$ fields. The adiabatic initial mixing and contour of the map are included with black dashed lines. The stoichiometric value is shown with a vertical line. Results for very advanced instants.

The relative position of the species does not change substantially with the ambient temperature. However, it is observed how for the 750 K case the partially premixed combustion is shifted to mixtures close to the stoichiometry and formaldehyde may be found at lean mixtures due to the high LOL value where combustion starts developing.

This section is closed with an analysis and discussion of the stabilization

mechanism of the flame and the apparition of ignition kernels in the LOL region. Experimental and modelling results evidence the role of auto-ignition as the main stabilization mechanism in diesel flames [57, 58, 59, 60] implying that this stabilization is strongly governed by chemistry.

Figure 13 shows the instantaneous temperature field for the cases of 750, 800 and 900 K in the region of the LOL for the modelled results for different instants. The figures include the instantaneous LOL value and the stoichiometric mixture fraction level curve. In addition, level curves for threshold values of ambient temperature plus 500 K are depicted for reference.

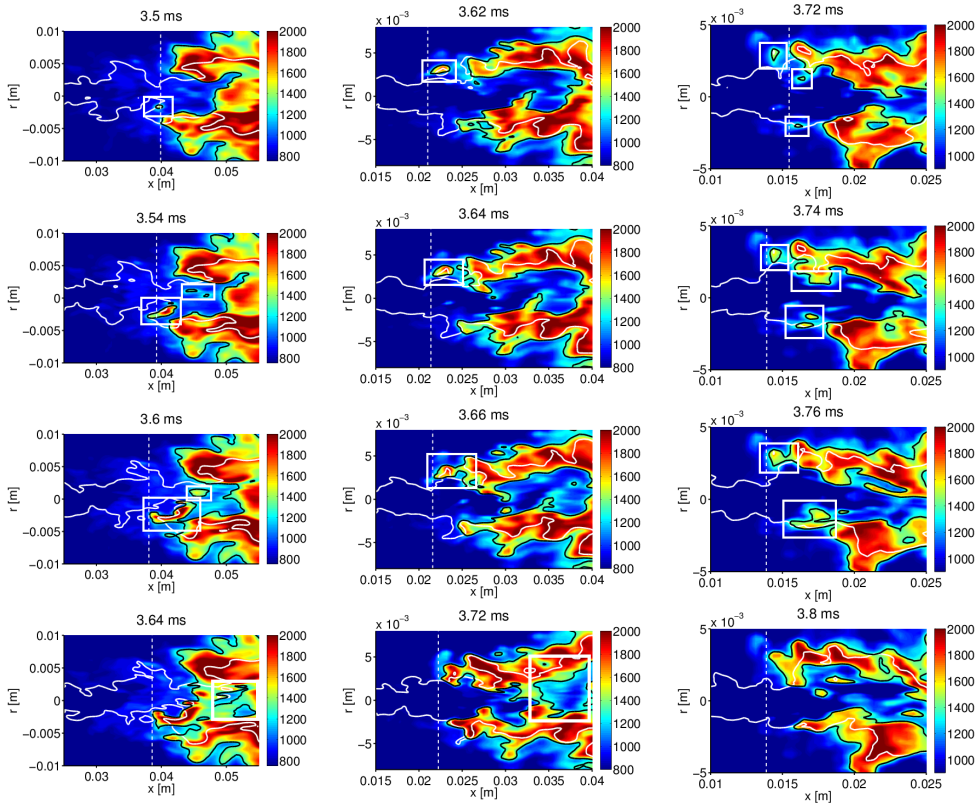

Figure 13: Instantaneous temperature fields for T_{amb} = 750 (left), 800 (center) and 900 K (right). Vertical white line shows the instantaneous LOL position while the solid white line indicates the stoichiometric level curve. Black lines are level curves for T_{amb} + 500 K.

The figures show how the level curves for temperature separate two zones

of unburned and burnt mixtures with a well-defined interface due to the sharp jump in the fields as a consequence of the high chemical source terms in the partially premixed combustion.

For the three temperatures it is observed how small ignition kernels appear in the vicinity of the LOL (for a better visualization different rectangles have been drawn surrounding some kernels). These pockets, which appear isolated and upstream of the main flame, increase in size and are convected downstream until they are brought close enough to get attached to the main flame. During the whole process the pocket expands over wider regions due to its growth to the surroundings as a consequence of the heat release and species diffusion until it merges with the base of the flame.

This phenomenology agrees with experimental observations where detached reactive pockets appearing upstream of the main flame were identified and led to conclude that the stabilization mechanism in a diesel flame is basically controlled by auto-ignition [57]. In addition, modelling works [59, 60] have reported similar observations about the formation of ignition kernels, their expansion and attachment to the main flame.

In addition, it is worth mentioning how pockets of unburned mixture are observed inside the flame as a consequence of its motion. It is observed how two branches of high temperature region get closer until they eventually merge and enclose a volume of fresh mixture. This is seen in the last instants for the cases 750 and 800 K in figure 13 where again for a better visualization these pockets have been enclosed in rectangles.

Finally, figure 13 shows clearly how the morphology of the base of the flame is drastically modified when changing the ambient temperature. Different to the nominal case, where two reactive lobes are clearly identified and the center of the flame remains inert, the 750 K case shows that the length of the lobes decrease while their width increase. Hence, reducing the ambient temperature provokes that the base of the flame becomes flatter.

3.2.3. Averaged fields

The analysis of the reactive spray is closed with a comparison of the averaged fields for the temperature sweep for very advanced instants. As the main aspects of the flame have been already described in the previous sections the spray behaviour is here briefly summarised. Some comments about the averaging process are first exposed.

One of the major difficulties in averaging the fields of diesel sprays is that even for the long time interval for which the simulation extends (4 ms) there exists a part of the head of the spray that is not in quasi-steady conditions. In addition, some fields like hydroxide found close to the stoichiometric level curve show strong variations complicating the averaging process.

In the current work, fields have been averaged in both azimuthal and temporal directions to obtain more representative averages. After checking, it was confirmed how 32 meridian planes are enough to reach convergence for the azimuthal averages. As the azimuthal average has slight effect on regions close to the axis and no effect on the axis, a temporal average is considered too. The window for averaging has been selected between 3.5 and 4 ms in order to consider a developed spray that extends in the wider possible region taking into account the limitations of the simulation.

As the spray shows a quasi-steady evolution [51], i.e. the spray fluid dynamics in a region stabilize rapidly once the spray passes through it, it is expected that representative averages are obtained in almost the whole spray and only the transient evolution affects the most advanced regions of the jet. Clearly, the representativeness of the average depends on the own nature of the field too, i.e. how the field changes with the mixture fraction, the scalar dissipation rate, etc.

The spatial averaged fields for the cases with ambient temperature 750, 800 and 900 K are shown in figure 14 for $\langle \widetilde{T} \rangle$, $\langle \widetilde{Y_{CH_2O}} \rangle$ and $\langle \widetilde{Y_{OH}} \rangle$ fields.

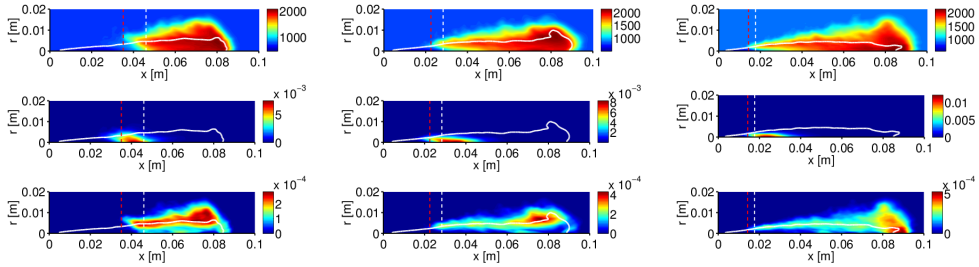

Figure 14: Averaged fields $\langle \widetilde{T} \rangle$ (first row), $\langle \widetilde{Y_{\mathrm{CH_2O}}} \rangle$ (second row) and $\langle \widetilde{Y_{\mathrm{OH}}} \rangle$ (third row) for 750 (left), 800 (center) and 900 K (right) cases. The averaged fields correspond to developed sprays. The level curve $\langle \widetilde{Z} \rangle = Z_{st}$ is included in white line. LOL values for experiment (white dashed) and simulation (red dashed) are shown too.

From figure 14 it is observed that the ambient temperature has a strong impact on the flame structure as expected. Reducing the ambient temperature moves the LOL downstream displacing, hence, the combustion to leaner mixtures and forcing that the whole combustion takes place in more reduced spatial regions since the stoichiometric level curve is closed at approximately the same distance from the nozzle for all the considered cases. The expected flame shape composed by two lobes is observed in all the cases although, as previously mentioned, this is not so clearly seen when reducing the ambient temperature since the displacement of the combustion downstream allows that the mixtures on the axis react at the same distance that the periphery of the spray.

As previously described, high concentrations of formaldehyde are observed in the vicinity of the LOL and enclosed in the region defined by the stoichiometric level curve, since this region corresponds to intermediate temperatures and rich mixtures. On the contrary, hydroxide is positioned on the stoichiometric level curve spreading in the slightly lean region where very high temperature values are reached.

The averages obtained by the method described previously generate fields that agree with those obtained by means of RANS simulations in other works [61, 10] and seem to converge for short and intermediate distances (until 60 mm). However, for larger distances, around 80 mm, it is probable that they have not converged completely as seen in the hydroxide field and the stoichiometric level

curve.

4. Conclusions and future work

Spray A from ECN has been modelled by means of LES simulations in inert and reactive conditions for an ambient temperature sweep. The dynamic structure model has been used for modelling the turbulence while a simplified approach to the flamelet concept together with a TCI description has been applied for the turbulent combustion evolution. A well-known chemical mechanism for the dodecane oxidation has been considered.

The inert spray has been calibrated in terms of vapour penetrations and mixture fraction and velocity fields. In addition, a satisfactory agreement has been obtained for the mixture fraction fluctuations. The spectral decomposition of the auto-correlation functions show that the LES simulations reproduce at least partially the inertial sub-range. In addition, the tip penetration and the velocity field for reactive conditions are properly described by the simulation. Finally, qualitative agreement is observed between CH_2O and OH fields for the reactive flame.

These positive results have encouraged an analysis of the reactive spray. The ID is well-captured except for very low ambient temperatures while the LOL trends, computed with two definitions, although being under-predicted, are correctly described. In addition, LOL has been shown to be subjected to a weak variability for all the cases, pointing in the direction that chemistry is intense enough to absorb the local dynamic flow fluctuations.

The instantaneous fields reproduce a partially premixed flame structure shaped in two lobes in the vicinity of the LOL followed by a diffusion flame established downstream where high temperature pockets are alternated by regions with lower temperatures as a consequence of the inhomogeneities that the turbulent flow induces. Formaldehyde is found in a close region to the LOL and the axis, showing some variability in Z-T maps, while hydroxide is positioned on the stoichiometric surface level and the lean side. The ambient temperature

has a strong effect on the position of the flame and, consequently, on the range of reactive mixtures with a clear impact on the soot formation. For the different boundary conditions it has been found that the ignition kernels appear in the proximity of the LOL, grow and merge with the main flame.

Averages have been carried out in azimuthal and temporal directions in order to filter the fluctuations related to the flow. An important fraction of the spray was correctly averaged because it reaches a quasi-steady regime and only at the head of the transient spray it was observed that the temporal interval was too short to provide representative averages. Moreover species with high variability appearing in the high temperature region, such as hydroxide, were especially difficult to average.

As a final conclusion, this work shows that the LES simulations provide reasonable results and the flamelet concept and, in particular, the ADF approach, has the ability to describe the flame structure accurately. This investigation encourages to analyse the influence of other parameters, such as the oxygen concentration, and to study in detail the stabilization flame mechanism.

5. Acknowledgements

Authors acknowledge that this work was possible thanks to the Ayuda para la Formación de Profesorado Universitario (FPU 14/03278) belonging to the Subprogramas de Formación y de Movilidad del Ministerio de Educación, Cultura y Deporte from Spain. Also this study was partially funded by the Ministerio de Economía y Competitividad from Spain in the frame of the COMEFF (TRA2014-59483-R) national project. Finally, the authors thankfully acknowledge the computer resources at MareNostrum and technical support provided by Barcelona Supercomputing Center (RES-FI-2017-2-0044).

References

[1] R. Novella, A. García, J. Pastor, V. Doménech, Mathematical and Computer Modelling 54 (2011) 1706–19.

[2] L. M. Pickett, G. Bruneaux, R. Payri, Sandia National Laboratories, Livermore, CA, https://ecn.sandia.gov/ (2019).

[3] N. Maes, M. Meijer, N. Dam, B. Somers, H. B. Toda, G. Bruneaux, S. Skeen, L. Pickett, J. Manin, Combustion and Flame 174 (2016) 138–51.

[4] M. Bardi, R. Payri, L. Malbec, G. Bruneaux, L. Pickett, J. Manin, T. Bazyn, C. L. Genzale, Atomization and Sprays 22 (2012).

[5] J. Benajes, R. Payri, M. Bardi, P. Martí-Aldaraví, Applied Thermal Engineering 58 (2013) 554–63.

[6] R. Payri, J. García-Oliver, T. Xuan, M. Bardi, Applied Thermal Engineering 90 (2015) 619–29.

[7] J. Desantes, J. García-Oliver, J. Pastor, A. Pandal, Atomization and Sprays 26 (2016).

[8] B. Naud, R. Novella, J. Pastor, J. Winklinger, Combustion and Flame 162 (2015) 893–906.

[9] Y. Pei, E. Hawkes, S. Kook, G. Goldin, T. Lu, Combustion and Flame 162 (2015) 2006–19.

[10] J. Desantes, J. García-Oliver, R. Novella, E. Pérez-Sánchez, Applied Thermal Engineering 117 (2017) 50–64.

[11] S. Pope, Turbulent flows, IOP Publishing, 2001.

[12] A. Kolmogorov 30 (1941) 299–303.

[13] S. Pope, New journal of Physics 6 (2004) 35.

[14] H. Pitsch, Annu. Rev. Fluid Mech. 38 (2006) 453–82.

[15] T. Poinsot, D. Veynante, Theoretical and numerical combustion, RT Edwards Inc., 2005.

[16] M. Germano, U. Piomelli, P. Moin, W. Cabot, Physics of Fluids A: Fluid Dynamics 3 (1991) 1760–5.

[17] A. Yoshizawa, K. Horiuti, Journal of the Physical Society of Japan 54 (1985) 2834–9.

[18] E. Pomraning, C. Rutland, AIAA journal 40 (2002) 689–701.

[19] N. Bharadwaj, C. Rutland, S. Chang, International Journal of Engine Research 10 (2009) 97–119.

[20] J. Mompó Laborda, Engineering Large Eddy Simulation of Diesel Sprays, Ph.D. thesis, Universitat Politècnica de València, 2014.

[21] J. v. Oijen, L. d. Goey, Combustion Science and Technology 161 (2000) 113–37.

[22] C. Pierce, P. Moin, Journal of fluid Mechanics 504 (2004) 73–97.

[23] M. Ihme, H. Pitsch, Combustion and flame 155 (2008) 70–89.

[24] M. Ihme, H. Pitsch, Combustion and flame 155 (2008) 90–107.

[25] J. Tillou, J. Michel, C. Angelberger, C. Bekdemir, D. Veynante, Oil & Gas Science and Technology-Revue de l'IFP 69 (2014) 155–65.

[26] F. Williams, Recent advances in theoretical descriptions of turbulent diffusion flames, Springer, 1975.

[27] N. Peters, Progress in Energy and Combustion Science 10 (1984) 319–39.

[28] N. Peters, Turbulent combustion, Cambridge University Press, 2000.

[29] H. Barths, C. Hasse, G. Bikas, N. Peters, Proceedings of the Combustion Institute 28 (2000) 1161–8.

[30] O. Gicquel, N. Darabiha, D. Thévenin, Proceedings of the Combustion Institute 28 (2000) 1901–8.

[31] J. Michel, O. Colin, D. Veynante, Combustion and Flame 152 (2008) 80–99.

[32] J. Michel, O. Colin, International Journal of Engine Research 15 (2014) 346–69.

[33] J. Tillou, J. Michel, C. Angelberger, D. Veynante, Combustion and Flame 161 (2014) 525–40.

[34] A. Kastengren, F. Tilocco, C. Powell, J. Manin, L. Pickett, R. Payri, T. Bazyn, Atomization and Sprays 22 (2012) 1011–52.

[35] Universitat Politècnica de València, Spain, http://www.cmt.upv.es/ECN03.aspx (2019).

[36] J. Pastor, J. Garcia-Oliver, J. Pastor, W. Vera-Tudela, Atomization and Sprays 25 (2015).

[37] http://www.openfoam.com/ (2019).

[38] P. Senecal, E. Pomraning, K. Richards, S. Som, SAE Technical Paper (2013).

[39] Q. Xue, S. Som, P. Senecal, E. Pomraning (2013).

[40] N. Bharadwaj, C. Rutland, Atomization and Sprays 20 (2010).

[41] J. Beale, R. Reitz, Atomization and sprays 9 (1999).

[42] http://www.reactiondesign.com/products/chemkin/ (2019).

[43] F. Payri, R. Novella, J. Pastor, E. Pérez-Sánchez, Applied Mathematical Modelling 49 (2017) 354–74.

[44] C. Pera, O. Colin, S. Jay, Oil & Gas Science and Technology-Revue de l'IFP 64 (2009) 243–58.

[45] K. Narayanaswamy, P. Pepiot, H. Pitsch, Combustion and Flame 161 (2014) 866–84.

[46] A. Frassoldati, G. D'Errico, T. Lucchini, A. Stagni, A. Cuoci, T. Faravelli, A. Onorati, E. Ranzi, Combustion and Flame 162 (2015) 3991–4007.

[47] B. Akkurt, H. Akargun, L. Somers, N. Deen, R. Novella, E. Pérez-Sánchez, SAE Technical Paper 2017-01-0577, 2017, doi:10.4271/2017-01-0577 (2017).

[48] L. Pickett, J. Manin, C. Genzale, D. Siebers, M. Musculus, C. Idicheria, SAE International Journal of Engines 4 (2011) 764–99.

[49] M. Meijer, L. Malbec, G. Bruneaux, L. Somers, in: 12th Triennial International Conference on Liquid Atomization and Spray Systems (ICLASS 2012), Heidelberg, Germany, September, pp. 2–6.

[50] W. Eagle, M. Musculus, L. Malbec, G. Bruneaux, in: ILASS Americas 26th Annual Conference on Liquid Atomization and Spray Systems, Portland, OR.

[51] J. García-Oliver, L. Malbec, H. Toda, G. Bruneaux, Combustion and Flame 179 (2017) 157–71.

[52] H. Tennekes, J. Lumley, A first course in turbulence, MIT press, 1972.

[53] S. Bhattacharjee, D. Haworth, Combustion and Flame 160 (2013) 2083–102.

[54] J. Dec, SAE Technical paper (1997).

[55] C. Duwig, L. Fuchs, Combustion Science and Technology 180 (2008) 453–80.

[56] E. Mastorakos, Progress in Energy and Combustion Science 35 (2009) 57–97.

[57] L. Pickett, D. Siebers, C. Idicheria, SAE technical paper (2005).

[58] C. Gong, M. Jangi, X. Bai, Applied Energy 136 (2014) 373–81.

[59] Y. Pei, S. Som, E. Pomraning, P. Senecal, S. Skeen, J. Manin, L. Pickett, Combustion and Flame 162 (2015) 4442–55.

[60] H. Kahila, A. Wehrfritz, O. Kaario, M. Masouleh, N. Maes, B. Somers, V. Vuorinen, Combustion and Flame 191 (2018) 142–59.

[61] Y. Pei, E. R. Hawkes, M. Bolla, S. Kook, G. M. Goldin, Y. Yang, S. Pope, S. Som, Combustion and Flame 168 (2016) 420–35.